

FineTec: Fine-Grained Action Recognition Under Temporal Corruption via Skeleton Decomposition and Sequence Completion

Dian Shao^{1*}, Mingfei Shi¹, Like Liu²

¹Unmanned System Research Institute, Northwestern Polytechnical University, Xi'an, China

²School of Software, Northwestern Polytechnical University, Xi'an, China

shaodian@nwpu.edu.cn, {mingfeishi5, like.liu}@mail.nwpu.edu.cn

Abstract

Recognizing fine-grained actions from temporally corrupted skeleton sequences remains a significant challenge, particularly in real-world scenarios where online pose estimation often yields substantial missing data. Existing methods often struggle to accurately recover temporal dynamics and fine-grained spatial structures, resulting in the loss of subtle motion cues crucial for distinguishing similar actions. To address this, we propose **FineTec**, a unified framework for Fine-grained action recognition under Temporal Corruption. FineTec first restores a base skeleton sequence from corrupted input using context-aware completion with diverse temporal masking. Next, a skeleton-based spatial decomposition module partitions the skeleton into five semantic regions, further divides them into dynamic and static subgroups based on motion variance, and generates two augmented skeleton sequences via targeted perturbation. These, along with the base sequence, are then processed by a physics-driven estimation module, which utilizes Lagrangian dynamics to estimate joint accelerations. Finally, both the fused skeleton position sequence and the fused acceleration sequence are jointly fed into a GCN-based action recognition head. Extensive experiments on both coarse-grained (NTU-60, NTU-120) and fine-grained (Gym99, Gym288) benchmarks show that FineTec significantly outperforms previous methods under various levels of temporal corruption. Specifically, FineTec achieves top-1 accuracies of 89.1% and 78.1% on the challenging Gym99-severe and Gym288-severe settings, respectively, demonstrating its robustness and generalizability. Code and datasets could be found at <https://smartdianlab.github.io/projects-FineTec/>.

1 Introduction

Fine-grained action recognition (FAR) aims to identify human actions characterized by slight temporal variations and subtle semantic differences, making it a particularly challenging problem (Shao et al. 2020a). Skeleton-based representations have emerged as an effective modality for FAR due to their compactness and explicit focus on motion cues (Duan et al. 2022b). However, in complex scenarios such as gymnastics, e.g., “*salto forward stretched with 2 twists*” (Shao et al. 2020a), online pose estimation can suffer

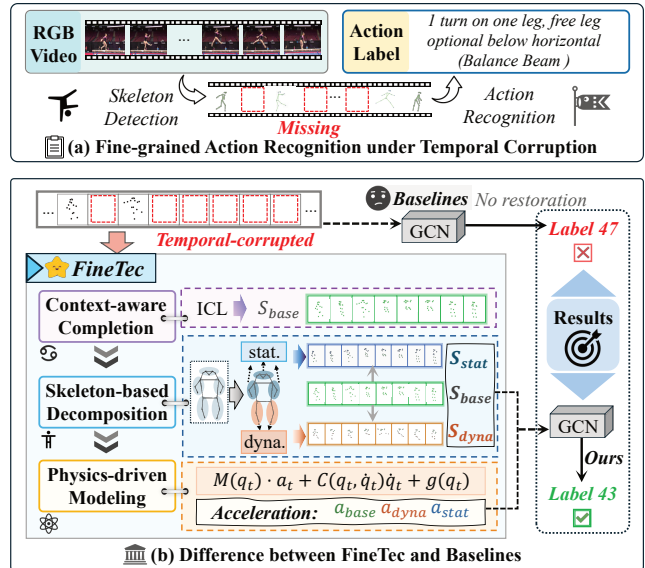


Figure 1: (a) Illustration of the challenging task: Fine-Grained Action Recognition under Temporal Corruption. (b) Compared to other GCN-based methods, the proposed FineTec framework can restore corrupted skeleton sequences and extract more discriminative features for recognition through context-aware completion, skeleton-based decomposition, and physics-driven modeling.

from severe frame dropping, reaching up to 69.6% dropping rate during rapid motion (Zheng et al. 2024). This results in temporally corrupted skeletal sequences and substantial performance degradation, as shown in Figure 1. The problem is especially critical for FAR, which depends on subtle, continuous motion cues (Huang et al. 2025; Myung et al. 2024) and is thus highly sensitive to temporal discontinuities.

Nevertheless, current skeleton-based approaches mainly face two limitations when handling FAR under temporal corruption: (1) inadequate temporal recovery, as most models are trained on clean, offline-annotated skeleton sequences and lack mechanisms to handle online detection artifacts (Liu et al. 2025; Jiang and Deng 2024; Xie et al. 2024); and (2) insufficient spatiotemporal modeling, as they often overlook the inherent biological structure of the hu-

*Corresponding author.

Copyright © 2026, Association for the Advancement of Artificial Intelligence (www.aaai.org). All rights reserved.

man body, focusing primarily on point-wise positional features while neglecting continuous kinematic constraints (Li et al. 2022; Leong et al. 2022; Chi et al. 2022).

To address these challenges, we introduce **FineTec**, a unified framework for **Fine**-grained action recognition under **Temporal Corruption**, as shown in Figure 2. Specifically, FineTec consists of three key modules: (1) The *Context-aware Sequence Completion* module restores severely corrupted skeleton sequences via diverse temporal masking and in-context learning strategies, enabling an approximate recovery of missing frames and temporal continuity. (2) The *Skeleton-based Spatial Decomposition* module partitions skeleton joints into five semantic regions based on biological priors, and further divides them into dynamic and static subgroups by motion variance. Targeted augmentation techniques are then applied within each subgroup to generate two sequences, amplifying fine-grained action distinctions. (3) The *Physics-driven Acceleration Modeling* module re-estimates joint accelerations at each time step using Lagrangian dynamics and pseudo-acceleration (computed as temporal differences between frames). The resulting acceleration sequences effectively capture discriminative motion cues essential for FAR. The whole process of how the skeleton sequence is restored, processed and utilized is illustrated in Figure 1. Finally, the fused skeleton sequence and its corresponding acceleration cues are integrated for action recognition via a GCN-based network.

To enable comprehensive evaluation, we construct the Gym288-skeleton dataset by extending the open-source Gym99. We manually annotate 11,000 initial-frame bounding boxes, apply OSTrack for athlete tracking, and perform pose estimation within the tracked boxes. The resulting dataset provides skeleton annotations for 288 fine-grained action classes, offering a more challenging benchmark for future research. To validate the effectiveness of FineTec, we conduct comprehensive experiments on both coarse-grained (NTU-60, NTU-120) and fine-grained (Gym99-skeleton, Gym288-skeleton) datasets, systematically simulating varying levels of temporal corruption, including minor (25% frame drop), moderate (50%), and severe (75%). Experimental results demonstrate that FineTec consistently outperforms previous methods across all settings, and maintains strong recognition accuracy even under severe frame-dropping scenarios.

Our contributions are summarized as follows:

- We formalize and benchmark fine-grained action recognition under temporal corruption, constructing a large-scale dataset, *Gym288-skeleton*, for comprehensive evaluation;
- We propose **FineTec**, a unified framework that integrates context-aware sequence completion, biologically-aware spatial decomposition, and physics-driven temporal refinement to recover corrupted temporal continuity and enhance skeleton sequence quality for improved recognition;
- Through extensive experiments on both coarse- and fine-grained datasets, we demonstrate that FineTec achieves state-of-the-art performance, especially in the presence of severe temporal corruption.

2 Related Work

Skeleton-based Fine-grained Action Recognition

Fine-grained Action Recognition (FAR) aims to distinguish subtle action differences (e.g., “pike sole circle backward with 0.5 turn to handstand”), enabling specialized analysis beyond coarse-grained categories (Zhang, Gupta, and Zisserman 2021; Yang et al. 2020; Wang et al. 2018; Chen et al. 2025; Shao et al. 2020b; Rajendran et al. 2024). Among modalities, skeletons provide an effective FAR representation by capturing human dynamics while avoiding background noise. And the key to FAR is enhancing distinctions in subtle motion details: MDR-GCN (Liu et al. 2023) and Sparse (Xie et al. 2025) enhance skeletal features multi-dimensionally. BlockGCN (Zhou et al. 2024) optimizes topological structure of GCNs to obtain more discriminative features. PoseConv3D (Duan et al. 2022b) employs a heatmap for spatio-temporal dynamics. PGVT (Zhang et al. 2024a) and SCoPLe (Zhu et al. 2025) integrates key-point with multi-modal features. However, they predominantly emphasize “displacement” information, relying on data-driven methods to implicitly learn complex temporal dynamics, and lacking guidance from physical realism. While ActCLR (Lin, Zhang, and Liu 2023) targets fine-grained resolution in skeletal space, its contrastive learning framework limits comprehensive exploitation. Diverging from prior work, FineTec enables physically interpretable modeling of fine-grained actions by concurrently addressing skeletal spatial granularity and physics-constrained temporal dynamics.

Physics-aware Video Understanding

Traditional video understanding is fundamentally limited by the agnostic nature of models and weakly interpretable feature spaces (Lin et al. 2025; Wang et al. 2025; Shao et al. 2025). And physics-aware manners (Gärtner et al. 2022a,b) offers a promising alternative by embedding physical principles. Some works leverage simulation environments for phenomena like rigid body collision or fluid dynamics (Andriluka et al. 2025; Liu et al. 2024), but adjusting physical parameters within engines remains challenging. Others directly integrate mathematical physics equations into model design (Zhang et al. 2024b; Ugrinovic et al. 2024). Among them, PIMNet (Zhang et al. 2022) uses Newtonian for motion prediction, InfoGCN++ (Chi et al. 2025) utilizes Neural-ODEs for action recognition, and LieGroupHamDL (Thai Duong and Atanasov 2023) combines Lie groups with Hamiltonian for robot control. In contrast, our FineTec: (1) focuses on fine-grained temporal-corrupted action recognition tasks; (2) introduces the ICL mechanism and masking strategies for temporal completion; (3) and integrates biological priors and Lagrangians for fine-grained analysis.

3 Methodology

Preliminary

□ **Physics of Rigid-body Dynamics.** Rigid-body dynamics are typically formulated using Lagrangian or Hamiltonian methods, with the Lagrangian formulation (Zhang,

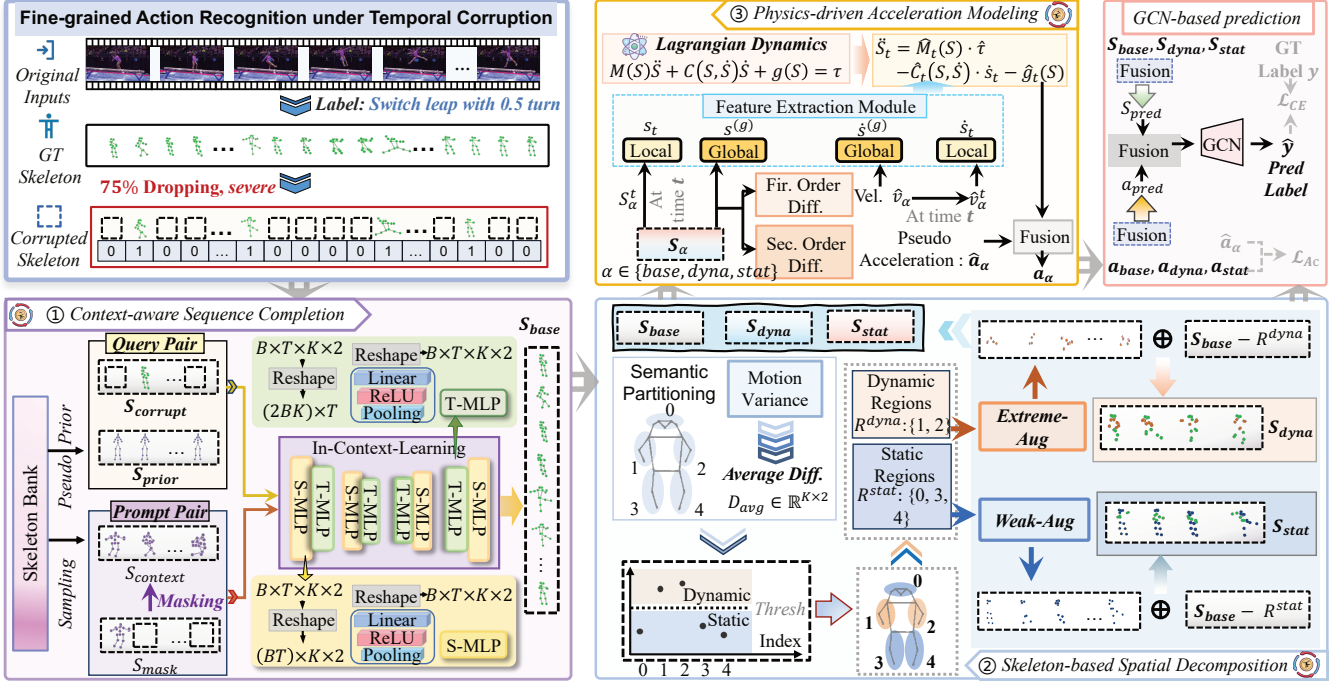


Figure 2: Overview of the Pipeline. FineTec consists of three core modules: ① Context-aware Sequence Completion restores missing or corrupted skeleton frames using in-context learning, producing S_{base} ; ② Skeleton-based Spatial Decomposition partitions S_{base} into anatomical regions by motion intensity, generating dynamic (S_{dyna}) and static (S_{stat}) variants, which are fused into S_{pred} ; ③ Physics-driven Acceleration Modeling infers joint accelerations via Lagrangian dynamics and data-driven finite differences, producing fused temporal dynamics features \mathbf{a} . The resulting positional (S_{pred}) and dynamic (a_{pred}) features are used for downstream fine-grained action recognition.

Kephart, and Ji 2024) widely adopted for its clarity and simplicity. For human kinematics (Jain and Rodriguez 1995), the Lagrangian dynamics are described by:

$$M(q_t) \cdot \ddot{q}_t + C(q_t, \dot{q}_t) \dot{q}_t + g(q_t) = \tau_t, \quad (1)$$

where q_t and \dot{q}_t denote generalized coordinates, at time t . $M(q_t)$ is the configuration-dependent inertia matrix reflecting the mass distribution of body segments; $C(q_t, \dot{q}_t) \dot{q}_t$ represents Coriolis and centrifugal forces; $g(q_t)$ accounts for gravitational forces; and τ_t denotes the vector of generalized forces, including joint torques and external influences.

○ Task Definition In this work, we address the challenging task of fine-grained action recognition under temporal corruption. Given a ground-truth 2D skeleton sequence $S_{gt} \in \mathbb{R}^{T \times K \times 2}$, where T is the number of frames and $K = 17$ is the number of joints, we simulate temporal corruption by randomly dropping 25% (minor), 50% (moderate), or 75% (severe) of the frames to obtain $S_{corrupt} \in \mathbb{R}^{T \times K \times D}$, with only $\hat{T} < T$ valid frames and the rest zero-padded. This setting reflects the missing data challenges frequently encountered in real-world online action detection scenarios. The goal is to predict the action category $y \in \{1, \dots, C\}$ from the corrupted sequence $S_{corrupt}$, where C is the number of action classes.

The FineTec Framework

○ Overall Pipeline. The FineTec framework processes temporally corrupted skeleton sequences through three key modules to achieve better fine-grained action recognition results, as illustrated in Figure 2. First, the *Context-aware Sequence Completion* module employs in-context learning to restore missing or corrupted frames, producing a basically completed skeleton sequence S_{base} . Next, the *Skeleton-based Spatial Decomposition* module partitions S_{base} into five anatomical regions and classifies them by motion intensity. Region-specific augmentations generate dynamic (S_{dyna}) and static (S_{stat}) variants, which are fused to yield the final sequence S_{pred} . These processed sequences are then used to extract displacement and acceleration features, which serve as inputs for downstream recognition networks. Finally, the *Physics-driven Acceleration Modeling* module infers joint accelerations via physics-based Lagrangian dynamics, and combine with data-driven finite differences to generate the fused temporal dynamics features \mathbf{a} . The resulting positional S_{pred} and dynamic features \mathbf{a} are then utilized together for downstream fine-grained action recognition.

♣ Context-aware Sequence Completion. To handle temporally corrupted skeleton sequences $S_{corrupt}$, we adopt an In-Context Learning (ICL) paradigm (Wang et al. 2024; Kim et al. 2025) to approximately recover the complete sequence

at first. We first construct a skeleton bank from Human3.6M 2D skeleton data, and obtain an average prior sequence S_{prior} via temporal averaging. For each training instance, a sequence is sampled from the bank and corrupted by one of five temporal masking strategies: random, pattern-based, or contiguous block masking (prefix, suffix, in-between). The original $S_{context}$ and the masked sequence S_{mask} form a prompt pair, demonstrating recovery from corruption. The input $S_{corrupt}$ is paired with S_{prior} as a query pair. Both the prompt and query pairs are processed by lightweight spatial and temporal MLPs, enabling the network to approximately restore the base sequence S_{base} by contextually completing missing frames. Further implementation details are provided in the Appendix.

♦ **Skeleton-based Spatial Decomposition.** This module enhances fine-grained action discrimination by decomposing and augmenting the predicted skeleton sequence S_{base} based on motion analysis and anatomical priors. Specifically, leveraging the human biological structure, we first partition the K joints into five semantic regions: head (G_0), left arm (G_1), right arm (G_2), left leg (G_3), and right leg (G_4). To quantify the motion level of each joint, we compute the average frame-wise displacement as follows:

$$D_{avg}^{(i)} = \frac{1}{T-1} \sum_{t=0}^{T-2} \|S_{base}^{t+1,i} - S_{base}^{t,i}\|_2 \quad (2)$$

where i indexes the joint. The regional motion intensity for each group G_j is then calculated as:

$$\bar{D}_j = \frac{1}{|G_j|} \sum_{i \in G_j} D_{avg}^{(i)} \in \mathbb{R}, \quad j \in \{G_1, G_2, \dots, G_5\}. \quad (3)$$

The top two regions with the highest \bar{D}_j are designated as dynamic, and the remaining three as static. To introduce region-specific diversity, we apply strong spatial-temporal perturbations (such as temporal cropping, random dropping, or interpolation) to S_{base} and selectively replace the *dynamic regions* with their perturbed versions, resulting in S_{dyna} . For static regions, we apply only weak spatial perturbations (e.g., random flipping) and substitute the corresponding *static regions* in S_{base} , producing S_{stat} .

Finally, S_{base} , S_{dyna} , and S_{stat} are fused to form the final sequence S_{pred} . This decomposition-augmentation-fusion strategy preserves temporal coherence, amplifies motion cues in dynamic regions, and stabilizes static postures, collectively improving fine-grained action recognition.

♥ **Physics-driven Acceleration Modeling.** In this module, we explicitly model acceleration dynamics using Lagrangian principles to enhance motion representation.

Recall the Lagrangian equation (Eq. 1), where we substitute the general coordinates q with the set of joint positions S :

$$M(S)\ddot{S} + C(S, \dot{S})\dot{S} + g(S) = \tau, \quad (4)$$

where M , C , g , and τ denote the inertia matrix, Coriolis matrix, gravity term, and driving force, respectively. Here

S could be S_{base} , S_{dyna} , and S_{stat} , and we omit the subscripts for convenience. Our aim is to calculate the acceleration term \ddot{S} :

$$\ddot{S} = \{M(S)\}^{-1} \cdot \tau - \hat{C}(S, \dot{S})\dot{S} - \hat{g}(S). \quad (5)$$

For computational efficiency and to facilitate neural network estimation, we define: $\hat{C}(S, \dot{S}) := M(S)^{-1}C(S, \dot{S})$, $\hat{g}(S) := M(S)^{-1}g(S)$, and $\hat{M}(S) := M(S)^{-1}$. To provide the necessary inputs for these estimators, we first extract both global and local features of the joint positions and velocities:

$$s^{(g)} = f_s^{(global)}(\{S^t\}_{t=0}^{T-1}), \quad s_t = f_s^{(local)}(S_t); \quad (6)$$

$$\dot{s}^{(g)} = f_{\dot{s}}^{(global)}(\{\dot{v}_t\}_{t=0}^{T-1}), \quad \dot{s}_t = f_{\dot{s}}^{(local)}(\dot{v}_t); \quad (7)$$

where \dot{v}_t is calculated using first-order finite differences as $\dot{v}_t = \frac{S_{t+1} - S_{t-1}}{2\Delta t}$. Each physical term in the dynamics equation is then estimated using neural networks \mathbb{E} . At a specific time t :

$$\hat{g}_t(S) = \mathbb{E}_g[s^{(g)}, s_t]. \quad (8)$$

Since τ is time-independent, we have:

$$\hat{\tau} = \mathbb{E}_\tau[\dot{s}^{(g)}, \dot{s}_t] \quad (9)$$

The remaining two terms are matrices, which we assume to be symmetric. Therefore, we first estimate their upper triangular parts and obtain the final matrices by applying the symmetry operation \mathcal{S}^\dagger :

$$\hat{C}_t(S, \dot{S}) = \mathcal{S}^\dagger \{\mathbb{E}_C[s^{(g)}, s_t, \dot{s}^{(g)}, \dot{s}_t]\}, \quad (10)$$

$$\hat{M}_t(S) = \mathcal{S}^\dagger \{\mathbb{E}_M[s^{(g)}, s_t]\}. \quad (11)$$

The refined, physics-driven acceleration is then computed as:

$$\ddot{S}_t = \hat{M}_t(S) \cdot \hat{\tau} - \hat{C}_t(S, \dot{S}) \cdot \dot{s}_t - \hat{g}_t(S). \quad (12)$$

To further improve robustness, we combine this estimate with the pseudo-acceleration calculated via second-order finite differences: $\hat{a}_t = \frac{S_{t+1} - 2S_t + S_{t-1}}{(\Delta t)^2}$. The final fused temporal dynamics feature (joint acceleration) is:

$$\mathbf{a}_t = \text{Fusion}(\hat{a}_t, \ddot{S}_t) \in \mathbb{R}^{K \times 2}. \quad (13)$$

♣ **GCN-based Optimization Objectives.** The FineTec framework is trained in two stages: skeleton sequence completion and the action recognition task.

① For sequence completion, we use mean squared error (MSE) losses to measure the difference between the completed skeleton and the ground-truth sequence, for both the prompt and query pairs:

$$\mathcal{L}_{ICL} = \text{MSE}(S_{gt}, S_{base}) + \text{MSE}(S_{context}, S_{mask}) \quad (14)$$

② For action recognition, the model utilizes the fused skeleton sequence S_{pred} and fused acceleration sequence \mathbf{a}_{pred} , which are integrated through a cross-attention module to capture both positional and dynamic information. The resulting representations are processed by graph convolutional

Method	Input	G288-Min.		G288-Mod.		G288-Sev.		G99-Min.		G99-Mod.		G99-Sev.	
		Top-1	Mean	Top-1	Mean	Top-1	Mean	Top-1	Mean	Top-1	Mean	Top-1	Mean
ST-GCN <i>AAAI'18</i>	Skeleton	0.784	0.381	0.770	0.344	0.742	0.304	0.895	0.869	0.876	0.829	0.871	0.783
PYSKL-J <i>arXiv'22</i>	Skeleton	0.813	0.401	0.794	0.368	0.773	0.315	0.920	0.871	0.903	0.856	0.884	0.791
PYSKL-B <i>arXiv'22</i>	Skeleton	0.811	0.385	0.796	0.373	0.765	0.314	0.915	0.872	0.905	0.858	0.889	0.801
PoseC3D-J <i>CVPR'22</i>	Heatmap	0.793	0.297	0.771	0.284	0.747	0.253	0.916	0.871	0.904	0.854	0.873	0.770
PoseC3D-L <i>CVPR'22</i>	Heatmap	0.790	0.296	0.775	0.281	0.756	0.250	0.917	0.870	0.899	0.848	0.870	0.761
AAGCN <i>TIP'20</i>	Skeleton	0.755	0.281	0.765	0.279	0.744	0.263	0.907	0.856	0.902	0.846	0.874	0.795
CTRGCN <i>ICCV'21</i>	Skeleton	0.786	0.292	0.784	0.285	0.760	0.271	0.914	0.874	0.897	0.859	0.884	0.803
Sparse <i>CVPR'25</i>	Skeleton	0.765	0.282	0.740	0.268	0.683	0.237	0.898	0.860	0.876	0.827	0.808	0.725
FineTec (Ours)	Skeleton	0.815	0.404	0.797	0.381	0.781	0.356	0.921	0.875	0.906	0.851	0.891	0.805

Table 1: Fine-grained action recognition on Gym99-skeleton and Gym288-skeleton. Both Top-1 accuracy and mean class accuracy are reported under minor (Min.), moderate (Mod.), and severe (Sev.) temporal corruption.

Method	NTU-60			NTU-120		
	Min.	Mod.	Sev.	Min.	Mod.	Sev.
ST-GCN	0.894	0.890	0.879	0.810	0.803	0.781
PYSKL-J	0.885	0.883	0.875	0.809	0.808	0.790
PYSKL-B	0.893	0.887	0.885	0.815	0.810	0.790
PoseC3D-J	0.887	0.889	0.878	0.823	0.795	0.783
PoseC3D-L	0.899	0.897	0.877	0.816	0.812	0.785
AAGCN	0.891	0.886	0.873	0.813	0.807	0.796
CTRGCN	0.901	0.892	0.879	0.814	0.809	0.793
Sparse	0.895	0.896	0.864	0.813	0.793	0.767
FineTec (Ours)	0.903	0.901	0.892	0.819	0.817	0.813

Table 2: Coarse-grained action recognition on NTU-60-xsub and NTU-120-xsub. Top-1 accuracy is reported under minor, moderate, and severe temporal corruption.

networks (GCNs) (Duan et al. 2022a), followed by a recognition head that predicts class probabilities \hat{y} . The classification loss is defined as the cross-entropy between the predicted and ground-truth labels:

$$\mathcal{L}_{CE} = - \sum_i y_i \log \hat{y}_i, \quad (15)$$

where y_i is the ground-truth label. An additional loss is also calculated between \hat{a} and a over the three sequences:

$$\mathcal{L}_{Ac} = \frac{1}{3} \sum_{\alpha} \text{MSE}(\hat{a}_{\alpha}, a_{\alpha}), \quad \alpha \in \{\text{base, dyna, stat}\}. \quad (16)$$

The overall training objective is:

$$\mathcal{L} = \mathcal{L}_{CE} + \lambda \mathcal{L}_{Ac}, \quad (17)$$

where λ is a balancing hyperparameter.

4 Experiment

Gym288-Skeleton Dataset

In this work, to enable comprehensive evaluation of fine-grained and temporally corrupted action recognition, we

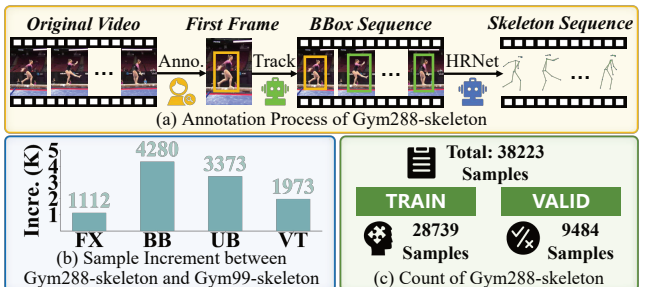


Figure 3: The Construction Process and Statistics of the constructed Gym288-skeleton Dataset.

construct the Gym288-skeleton dataset by extending the open-source Gym99 dataset. We manually annotate $\sim 1.1w$ initial-frame bounding boxes, apply OSTrack (Ye et al. 2022) for athlete tracking, and perform pose estimation within the tracked boxes for each video. This provides a large-scale dataset with skeleton annotations for 288 fine-grained action classes, advancing the scope and difficulty of existing benchmarks. Statistics are shown in Figure 3, and the detailed constructing process and analysis are shown in the supplementary material.

Evaluation Settings

» Datasets: We conduct fine-grained action recognition experiments on two benchmark datasets: Gym99-skeleton and the constructed Gym288-skeleton (Shao et al. 2020a). For coarse settings, we use the NTU datasets, including NTU60 (Shahroudy et al. 2016) and NTU120 (Liu et al. 2020).

» Baselines: We compare our method with several representative skeleton-based approaches: ST-GCN (Yan, Xiong, and Lin 2018), PYSKL (Duan et al. 2022a), PoseC3D (Duan et al. 2022b), AAGCN (Shi et al. 2020), CTRGCN (Chen et al. 2021), and Sparse (Xie et al. 2025).

» Evaluation Metrics: For action recognition, we report Top-1 and Top-5 accuracy. Due to the significant class imbalance in Gym288 (Shao et al. 2020a), Mean class accuracy (Mean) is also included as a more informative metric. For skeleton restoration, we employ standard metrics: Mean Per

Method	Gym99-Min.			Gym99-Mod.			Gym99-Sev.		
	MPJPE \downarrow	N-MPJPE \downarrow	MPJVE \downarrow	MPJPE \downarrow	N-MPJPE \downarrow	MPJVE \downarrow	MPJPE \downarrow	N-MPJPE \downarrow	MPJVE \downarrow
L-R Copy	0.136	0.133	0.246	0.332	0.318	0.445	0.713	0.665	0.575
R-L Copy	0.136	0.132	0.246	0.327	0.313	0.441	0.699	0.650	0.571
siMLPe	0.175	0.139	0.119	0.208	0.168	0.129	0.245	0.199	0.139
SiC-Stat	0.210	0.102	0.351	0.397	0.181	0.508	0.584	0.252	0.544
SiC-Dyna	0.188	0.100	0.196	0.164	0.144	0.205	0.192	0.174	0.321
Ours	0.106	0.098	0.047	0.119	0.109	0.085	0.147	0.132	0.113

Table 3: Skeleton restoration results on Gym99-Skeleton. Experiments are conducted under three levels of temporal corruption: minor, moderate, and severe. The evaluation metrics include MPJPE, N-MPJPE, and MPJVE. And the “L-R” and “R-L” denote left-to-right and right-to-left respectively.

Index	Cont.	Skel.	Phys.	Minor	Moderate	Severe
❶	\times	✓	✓	0.812	0.785	0.751
❷	✓	\times	✓	0.787	0.780	0.770
❸	✓	✓	\times	0.789	0.776	0.775
❹	✓	✓	✓	0.815	0.797	0.781

Table 4: Ablations of different modules, including the Context-aware Sequence Completion (Cont.), Skeleton-based Spatial Decomposition (Skel.), and Physics-driven Acceleration Modeling (Phys.).

Index	S_{dyna}	S_{stat}	Moderate	Severe
❶	\times	✓	0.790	0.774
❷	✓	\times	0.786	0.764
❸	✓	✓	0.797	0.781

Table 5: Analysis on augmented skeleton sequences.

Joint Position Error (MPJPE) and Mean Per Vertex Position Error (MPVPE). Main results are presented in this section, with further details provided in the Appendix.

Main Results

Results on Fine-grained Action Recognition. The main quantitative results on the two fine-grained skeleton datasets, Gym99 and Gym288-skeleton, are presented in Table 1. These results are reported across three difficulty levels: minor (25% frame missing), moderate (50% frame missing), and severe (75% frame missing). It can be observed that the proposed FineTec framework consistently achieves the best performance under all conditions. Notably, in the most challenging scenario—Gym288-skeleton with severe frame missing—FineTec attains a Top-1 accuracy of 78.1%, surpassing all previous skeleton-based methods. In terms of mean class accuracy, FineTec improves upon the best baseline by 13%, and outperforms the latest work (Xie et al. 2025) by 50%. Overall, these results demonstrate that FineTec achieves outstanding effectiveness across fine-grained datasets and under all levels of difficulty.

Results on Coarse-grained Action Recognition. To further evaluate the generalization and robustness of FineTec, we conduct experiments on the coarse-grained skeleton action

recognition benchmarks, including NTU-60-xsub and NTU-120-xsub, and UCF101 (Soomro, Zamir, and Shah 2012). The results are shown in Table 2, showing that FineTec outperforms all competitive baselines, particularly under the most challenging (severe) condition, achieving Top-1 accuracy improvements of 1.3% on NTU-60-xsub and 1.7% on NTU-120-xsub. Results on UCF101 are provided in the Appendix due to space limitations.

Main Results on Skeleton Restoration. We quantitatively evaluate the ability of FineTec to restore temporally corrupted skeleton sequences, as presented in Table 3. Notably, our method achieves the lowest MPJPE across all corruption levels, substantially outperforming all baselines. Compared to the strongest competing method (SiC-Dyna), MaskICL achieves MPJPE reductions of 43.6% under minor corruption, 27.4% under moderate corruption, and 23.4% under severe corruption. Consistent improvements are also observed for N-MPJPE and MPJVE, where our method achieves the best performance across all settings.

Ablations and Analysis

Ablation Studies of Modules. We validate FineTec’s design through ablation studies of its three main modules and their variants on the Gym288-skeleton dataset, evaluated in terms of top-1 accuracy. **❶** Module Ablation: Table 4 demonstrates that removing any FineTec module results in a clear performance drop, confirming the necessity of each component and the effectiveness of the overall design. **❷** Analysis of Skeleton Decomposition: Table 5 shows that combining both S_{dyna} and S_{stat} achieves higher accuracy than using either alone, demonstrating that spatial decomposition and differentiated processing enrich skeleton features and enhance fine-grained action recognition. **❸** Fusion Strategy in Physics-driven module: We compare cross-attention (CA) fusion and MLP-based integration for integrating acceleration cues. CA consistently outperforms MLP in both moderate (0.797 vs. 0.779) and severe (0.781 vs. 0.771) settings (Top-1 Acc.), validating the effectiveness of the selected fusion strategy.

Impact of Sequence Completion on Action Recognition. We investigate how different sequence completion methods affect fine-grained action recognition accuracy, as shown in

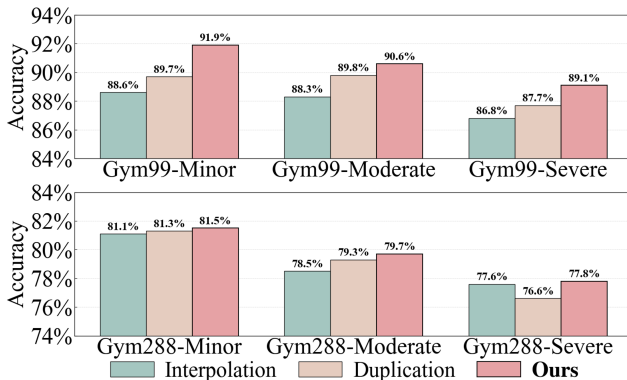


Figure 4: Comparison of Skeleton Restoration Methods on Gym99-skeleton and Gym288-skeleton. Top-1 accuracy of FineTec (Ours), Interpolation, and Duplication is reported under varying levels of temporal corruption.

Perturb.	G99-Min.	G99-Sev.	G288-Min.	G288-Sev.
S-low	0.91/0.985	0.842/0.971	0.790/0.911	0.764/0.905
S-high	0.900/0.983	0.825/0.967	0.785/0.908	0.736/0.884
T-low	0.898/0.988	0.869/0.981	0.791/0.918	0.777/0.915
T-high	0.896/0.987	0.862/0.979	0.789/0.917	0.774/0.914
w/o	0.926/0.995	0.896/0.988	0.819/0.928	0.804/0.924

Table 6: Robustness analysis under spatial and temporal perturbations. Yellow rows indicate spatial (Gaussian noise) perturbations, and blue rows indicate temporal (frame dropping) perturbations. Top-1 / Top-5 accuracy are reported.

Figure 4. Compared to standard approaches such as Interpolation and Duplication, FineTec consistently yields the highest Top-1 accuracy on both fine-grained action recognition datasets, across varying levels of temporal degradation. Specifically, on the Gym99 dataset, FineTec achieves Top-1 accuracies of 0.919 (minor), 0.906 (moderate), and 0.885 (severe), demonstrating notable robustness even under significant data loss. The improvements are even more pronounced on the more challenging Gym288 dataset, where FineTec attains Top-1 accuracies of 0.815 (minor), 0.797 (moderate), and 0.778 (severe), outperforming all baselines. In particular, under severe degradation, FineTec significantly surpasses both Duplication and Interpolation. These results show that effective sequence completion significantly benefits action recognition under temporal corruption.

Qualitative Visualization of Skeleton Restoration. Figure 5 presents a qualitative comparison of skeleton sequence restoration for a sample from the Gym288 dataset (Label 122: “*Salto backward stretched with 1.5 twist*”) under severe corruption. We compare our context-aware completion module with an ablation variant that excludes in-context learning. Both methods use identical training settings, yet our approach better reconstructs the missing frames and preserves the fine-grained motion details.

Robustness to Noisy Inputs. We assess the robustness of FineTec under both spatial and temporal perturbations. Spa-

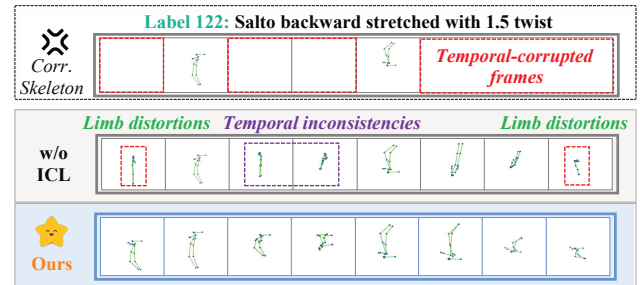


Figure 5: Qualitative Results of Skeleton Restoration. Our context-aware completion method more accurately reconstructs missing frames and preserves fine-grained motion details compared to the ablation without in-context learning.

tial noise is introduced by adding Gaussian noise at two severity levels (“S-low” and “S-high”). Temporal robustness is evaluated by randomly dropping half of the input frames, also at two severity levels (“T-low” and “T-high”). As summarized in Table 6, FineTec maintains high recognition accuracy under all perturbations. These results demonstrate FineTec’s strong resilience to both spatial and temporal input corruptions, ensuring reliable performance even in challenging real-world scenarios.

Discussion and Future Works. FineTec establishes a strong foundation for robust fine-grained action recognition under temporal corruption, demonstrating the potential of detailed spatio-temporal and physics-driven modeling. Building on this foundation, there remain many promising directions for future research. For example, the current use of a fixed skeleton bank in sequence completion and manually defined subgroup partitioning can inspire future work on more adaptive, data-driven approaches. Additionally, extending our joint-level acceleration modeling to subgroup or limb-level dynamics may further enrich the model’s understanding of human motion. We believe these directions, building on the foundation established by FineTec, will drive continued progress in robust action recognition.

5 Conclusion

In this work, we tackle the challenging problem of fine-grained action recognition under temporal corruption. We introduce FineTec, a unified framework specifically designed to address this issue. FineTec first restores temporal continuity from corrupted inputs via a Context-aware Sequence Completion module. It then employs Skeleton-based Spatial Decomposition, guided by biological priors, to partition the skeleton and amplify subtle motion distinctions. Finally, a Physics-driven Acceleration Modeling module leverages Lagrangian dynamics to capture discriminative motion cues beyond simple displacement. Extensive experiments on both coarse-grained and fine-grained benchmarks demonstrate that FineTec consistently outperforms existing methods under varying degrees of temporal corruption. Future directions involve expanding our framework to multi-modal contexts and enhancing biomechanical modeling.

6 Acknowledgments

This work was funded by the National Natural Science Foundation of China (NSFC) under Grant 62306239, and supported by the Sanqin Talents Introduction Plan of Shaanxi Province, China.

References

Andriluka, M.; Tabanpour, B.; Freeman, C. D.; and Sminchisescu, C. 2025. Learned Neural Physics Simulation for Articulated 3D Human Pose Reconstruction. In Leonardis, A.; Ricci, E.; Roth, S.; Russakovsky, O.; Sattler, T.; and Varol, G., eds., *Computer Vision – ECCV 2024*, 320–336. Cham: Springer Nature Switzerland. ISBN 978-3-031-72907-2.

Chen, H.; Huang, H.; Yin, X.; and Shao, D. 2025. FineQuest: Adaptive Knowledge-Assisted Sports Video Understanding via Agent-of-Thoughts Reasoning. In *Proceedings of the 33rd ACM International Conference on Multimedia*, MM '25, 2909–2918. New York, NY, USA: Association for Computing Machinery. ISBN 9798400720352.

Chen, Y.; Zhang, Z.; Yuan, C.; Li, B.; Deng, Y.; and Hu, W. 2021. Channel-wise topology refinement graph convolution for skeleton-based action recognition. In *Proceedings of the IEEE/CVF international conference on computer vision*, 13359–13368.

Chi, H.-g.; Ha, M. H.; Chi, S.; Lee, S. W.; Huang, Q.; and Ramani, K. 2022. Infogcn: Representation learning for human skeleton-based action recognition. In *Proceedings of the IEEE/CVF conference on computer vision and pattern recognition*, 20186–20196.

Chi, S.; Chi, H.-G.; Huang, Q.; and Ramani, K. 2025. InfoGCN++: Learning Representation by Predicting the Future for Online Skeleton-Based Action Recognition. *IEEE Transactions on Pattern Analysis & Machine Intelligence*, 47(01): 514–528.

Duan, H.; Wang, J.; Chen, K.; and Lin, D. 2022a. Pyskl: Towards good practices for skeleton action recognition. In *Proceedings of the 30th ACM International Conference on Multimedia*, 7351–7354.

Duan, H.; Zhao, Y.; Chen, K.; Lin, D.; and Dai, B. 2022b. Revisiting skeleton-based action recognition. In *Proceedings of the IEEE/CVF conference on computer vision and pattern recognition*, 2969–2978.

Gärtner, E.; Andriluka, M.; Coumans, E.; and Sminchisescu, C. 2022a. Differentiable dynamics for articulated 3d human motion reconstruction. In *Proceedings of the IEEE/CVF conference on computer vision and pattern recognition*, 13190–13200.

Gärtner, E.; Andriluka, M.; Xu, H.; and Sminchisescu, C. 2022b. Trajectory optimization for physics-based reconstruction of 3d human pose from monocular video. In *Proceedings of the IEEE/CVF Conference on Computer Vision and Pattern Recognition*, 13106–13115.

Huang, Y.; Chen, H.; Xu, Z.; Jia, Z.; Sun, H.; and Shao, D. 2025. SeFAR: Semi-supervised Fine-grained Action Recognition with Temporal Perturbation and Learning Stabilization. *arXiv preprint arXiv:2501.01245*.

Ionescu, C.; Papava, D.; Olaru, V.; and Sminchisescu, C. 2014. Human3.6M: Large Scale Datasets and Predictive Methods for 3D Human Sensing in Natural Environments. *IEEE Transactions on Pattern Analysis and Machine Intelligence*, 36(7): 1325–1339.

Jain, A.; and Rodriguez, G. 1995. Diagonalized Lagrangian robot dynamics. *IEEE Transactions on Robotics and Automation*, 11(4): 571–584.

Jiang, Y.; and Deng, H. 2024. Lighter and faster: A multi-scale adaptive graph convolutional network for skeleton-based action recognition. *Engineering Applications of Artificial Intelligence*, 132: 107957.

Kim, K.; Park, G.; Lee, Y.; Yeo, W.; and Hwang, S. J. 2025. VideoICL: Confidence-based Iterative In-context Learning for Out-of-Distribution Video Understanding. In *Proceedings of the Computer Vision and Pattern Recognition Conference*, 3295–3305.

Leong, M. C.; Zhang, H.; Tan, H. L.; Li, L.; and Lim, J. H. 2022. Combined CNN transformer encoder for enhanced fine-grained human action recognition. *arXiv preprint arXiv:2208.01897*.

Li, T.; Foo, L. G.; Ke, Q.; Rahmani, H.; Wang, A.; Wang, J.; and Liu, J. 2022. Dynamic spatio-temporal specialization learning for fine-grained action recognition. In *European Conference on Computer Vision*, 386–403. Springer.

Lin, L.; Zhang, J.; and Liu, J. 2023. Actionlet-dependent contrastive learning for unsupervised skeleton-based action recognition. In *Proceedings of the IEEE/CVF Conference on Computer Vision and Pattern Recognition*, 2363–2372.

Lin, M.; Wang, X.; Wang, Y.; Wang, S.; Dai, F.; Ding, P.; Wang, C.; Zuo, Z.; Sang, N.; Huang, S.; et al. 2025. Exploring the evolution of physics cognition in video generation: A survey. *arXiv preprint arXiv:2503.21765*.

Liu, H.; Liu, Y.; Ren, M.; Wang, H.; Wang, Y.; and Sun, Z. 2025. Revealing key details to see differences: A novel prototypical perspective for skeleton-based action recognition. In *Proceedings of the Computer Vision and Pattern Recognition Conference*, 29248–29257.

Liu, J.; Shahroudy, A.; Perez, M.; Wang, G.; Duan, L.-Y.; and Kot, A. C. 2020. NTU RGB+D 120: A large-scale benchmark for 3D human activity understanding. *IEEE Transactions on Pattern Analysis and Machine Intelligence*, 42(10): 2684–2701.

Liu, S.; Ren, Z.; Gupta, S.; and Wang, S. 2024. Physgen: Rigid-body physics-grounded image-to-video generation. In *European Conference on Computer Vision*, 360–378. Springer.

Liu, S.-L.; Ding, Y.-N.; Zhang, J.-R.; Liu, K.-Y.; Zhang, S.-F.; Wang, F.-L.; and Huang, G. 2023. Multi-Dimensional Refinement Graph Convolutional Network with Robust Decouple Loss for Fine-Grained Skeleton-Based Action Recognition. *arXiv:2306.15321*.

Myung, W.; Su, N.; Xue, J.-H.; and Wang, G. 2024. Degen: Deformable graph convolutional networks for skeleton-based action recognition. *IEEE Transactions on Image Processing*, 33: 2477–2490.

Rajendran, M.; Tan, C. T.; Atmosukarto, I.; Ng, A. B.; and See, S. 2024. Review on synergizing the Metaverse and AI-driven synthetic data: enhancing virtual realms and activity recognition in computer vision. *Visual Intelligence*, 2(1): 27.

Shahroudy, A.; Liu, J.; Ng, T.-T.; and Wang, G. 2016. NTU RGB+D: A large scale dataset for 3D human activity analysis. In *CVPR*, 1010–1019.

Shao, D.; Shi, M.; Xu, S.; Chen, H.; Huang, Y.; and Wang, B. 2025. FinePhys: Fine-grained Human Action Generation by Explicitly Incorporating Physical Laws for Effective Skeletal Guidance. In *Proceedings of the IEEE/CVF Conference on Computer Vision and Pattern Recognition*, 1905–1916.

Shao, D.; Zhao, Y.; Dai, B.; and Lin, D. 2020a. Finegym: A hierarchical video dataset for fine-grained action understanding. In *Proceedings of the IEEE/CVF conference on computer vision and pattern recognition*, 2616–2625.

Shao, D.; Zhao, Y.; Dai, B.; and Lin, D. 2020b. Intra-and inter-action understanding via temporal action parsing. In *Proceedings of the IEEE/CVF conference on computer vision and pattern recognition*, 730–739.

Shi, L.; Zhang, Y.; Cheng, J.; and Lu, H. 2020. Skeleton-based action recognition with multi-stream adaptive graph convolutional networks. *IEEE Transactions on Image Processing*, 29: 9532–9545.

Soomro, K.; Zamir, A. R.; and Shah, M. 2012. UCF101: A Dataset of 101 Human Actions Classes From Videos in The Wild. *Computer Science*.

Sun, K.; Xiao, B.; Liu, D.; and Wang, J. 2019. Deep High-Resolution Representation Learning for Human Pose Estimation. In *CVPR*.

Thai Duong, J. S., Abdullah Altawaitan; and Atanasov, N. 2023. Port-Hamiltonian Neural ODE Networks on Lie Groups For Robot Dynamics Learning and Control. *arXiv preprint arXiv:2401.09520*.

Ugrinovic, N.; Pan, B.; Pavlakos, G.; Paschalidou, D.; Shen, B.; Sanchez-Riera, J.; Moreno-Noguer, F.; and Guibas, L. 2024. Multiphys: Multi-person physics-aware 3d motion estimation. In *Proceedings of the IEEE/CVF Conference on Computer Vision and Pattern Recognition*, 2331–2340.

Wang, L.; Xiong, Y.; Wang, Z.; Qiao, Y.; Lin, D.; Tang, X.; and Van Gool, L. 2018. Temporal segment networks for action recognition in videos. *IEEE transactions on pattern analysis and machine intelligence*, 41(11): 2740–2755.

Wang, M.; Huang, Z.; Kong, X.; Shen, G.; Dai, G.; Wang, J.; and Liu, Y. 2025. Action Detail Matters: Refining Video Recognition with Local Action Queries. In *Proceedings of the Computer Vision and Pattern Recognition Conference*, 19132–19142.

Wang, X.; Fang, Z.; Li, X.; Li, X.; Chen, C.; and Liu, M. 2024. Skeleton-in-context: Unified skeleton sequence modeling with in-context learning. In *Proceedings of the IEEE/CVF Conference on Computer Vision and Pattern Recognition*, 2436–2446.

Xie, J.; Meng, Y.; Zhao, Y.; Nguyen, A.; Yang, X.; and Zheng, Y. 2024. Dynamic semantic-based spatial graph convolution network for skeleton-based human action recognition. In *Proceedings of the AAAI conference on artificial intelligence*, volume 38, 6225–6233.

Xie, J.; Zhao, Y.; Meng, Y.; Zhao, H.; Nguyen, A.; and Zheng, Y. 2025. Are Spatial-Temporal Graph Convolution Networks for Human Action Recognition Over-Parameterized? In *CVPR*, 24309–24319.

Yan, S.; Xiong, Y.; and Lin, D. 2018. Spatial temporal graph convolutional networks for skeleton-based action recognition. In *Proceedings of the AAAI conference on artificial intelligence*, volume 32.

Yang, C.; Xu, Y.; Shi, J.; Dai, B.; and Zhou, B. 2020. Temporal pyramid network for action recognition. In *Proceedings of the IEEE/CVF conference on computer vision and pattern recognition*, 591–600.

Ye, B.; Chang, H.; Ma, B.; Shan, S.; and Chen, X. 2022. Joint Feature Learning and Relation Modeling for Tracking: A One-Stream Framework. In *ECCV*.

Zhang, C.; Gupta, A.; and Zisserman, A. 2021. Temporal query networks for fine-grained video understanding. In *Proceedings of the ieee/cvf conference on computer vision and pattern recognition*, 4486–4496.

Zhang, H.; Leong, M. C.; Li, L.; and Lin, W. 2024a. PGVT: Pose-Guided Video Transformer for Fine-Grained Action Recognition. In *2024 IEEE/CVF Winter Conference on Applications of Computer Vision (WACV)*, 6631–6642.

Zhang, Y.; Kephart, J. O.; Cui, Z.; and Ji, Q. 2024b. Physpt: Physics-aware pretrained transformer for estimating human dynamics from monocular videos. In *Proceedings of the IEEE/CVF Conference on Computer Vision and Pattern Recognition*, 2305–2317.

Zhang, Y.; Kephart, J. O.; and Ji, Q. 2024. Incorporating Physics Principles for Precise Human Motion Prediction. In *Proceedings of the IEEE/CVF Winter Conference on Applications of Computer Vision (WACV)*, 6164–6174.

Zhang, Z.; Zhu, Y.; Rai, R.; and Doermann, D. 2022. PIM-Net: Physics-Infused Neural Network for Human Motion Prediction. *IEEE Robotics and Automation Letters*, 7(4): 8949–8955.

Zheng, G.; Lin, S.; Zuo, H.; Fu, C.; and Pan, J. 2024. Net-track: Tracking highly dynamic objects with a net. In *Proceedings of the IEEE/CVF Conference on Computer Vision and Pattern Recognition*, 19145–19155.

Zhou, Y.; Yan, X.; Cheng, Z.-Q.; Yan, Y.; Dai, Q.; and Hua, X.-S. 2024. BlockGCN: Redefining Topology Awareness for Skeleton-Based Action Recognition. In *Proceedings of the IEEE/CVF Conference on Computer Vision and Pattern Recognition*.

Zhu, A.; Zhu, J.; Bailey, J.; Gong, M.; and Ke, Q. 2025. Semantic-guided Cross-Modal Prompt Learning for Skeleton-based Zero-shot Action Recognition. In *Proceedings of the Computer Vision and Pattern Recognition Conference*, 13876–13885.

A Training & Dataset Details

Overview

We deploy FineTec using PyTorch, and the training process consists of two steps: ① Pre-train the Context-aware Sequence Completion module on skeletal datasets; ② Train the FineTec framework, while keeping the Completion module frozen.

For the initial pre-training phase of the Context-aware Sequence Completion module on skeletal datasets, the training regimen in Gym99 and Gym288-skeleton datasets is established as follows. The model processes input sequences of 16 frames. Each frame's representation is a concatenation of 34-dimensional skeletal features, a 1-dimensional mask indicator, and 8-dimensional positional encodings, yielding a 43-dimensional input per frame. Meanwhile, skeletons from Human3.6M datasets (Ionescu et al. 2014) are utilized to form both query-prior and in-context pairs, which are processed into the backbone. The core network architecture is a 48-layer S-MLPs and T-MLPs incorporating normalization. An input fully connected layer maps the 43-dimensional frame-wise input to an internal embedding dimension of 34, employing a ReLU activation. Subsequently, an output fully connected layer projects the processed embeddings back to the 34-dimensional skeletal feature space, also utilizing ReLU activation, and its weights are initialized using a truncated normal distribution.

For the second training stage, where FineTec is trained while the parameters of the pre-trained Context-aware Sequence Completion module are kept frozen, we configure the training process as follows. Optimization is conducted using the Stochastic Gradient Descent (SGD) algorithm, incorporating Nesterov momentum. The optimizer is initialized with a learning rate from 0.05 to 0.2, a momentum coefficient of 0.9, and an L2 weight decay of (5×10^{-4}) . To dynamically adjust the learning rate, a cosine annealing schedule is applied over 200 epochs, reducing the learning rate to a minimum of 0.

In terms of both NTU-60-xsub (Shahroudy et al. 2016) and NTU-120-xsub (Liu et al. 2020) skeleton datasets, the input sequence length is set to 100 frames. And skeletons in Human3.6M are also sampled with 100 frames.

Context-aware Sequence Completion Module Pre-training

The training is performed with a batch size of 256, supported by 8 data loader workers. Optimization is carried out using an Adam optimizer, governed by a cosine annealing learning rate schedule. The learning rate cycles between a maximum of (1×10^{-5}) and a minimum of (5×10^{-8}) over a total of 40,000 iterations. A weight decay of (1×10^{-4}) is applied for regularization. To enhance model robustness, data augmentation techniques are utilized. Furthermore, the model is configured to process derivative information from both input and output signals, potentially capturing velocity or acceleration dynamics. All experiments are conducted with a fixed random seed of 304 to ensure reproducibility.

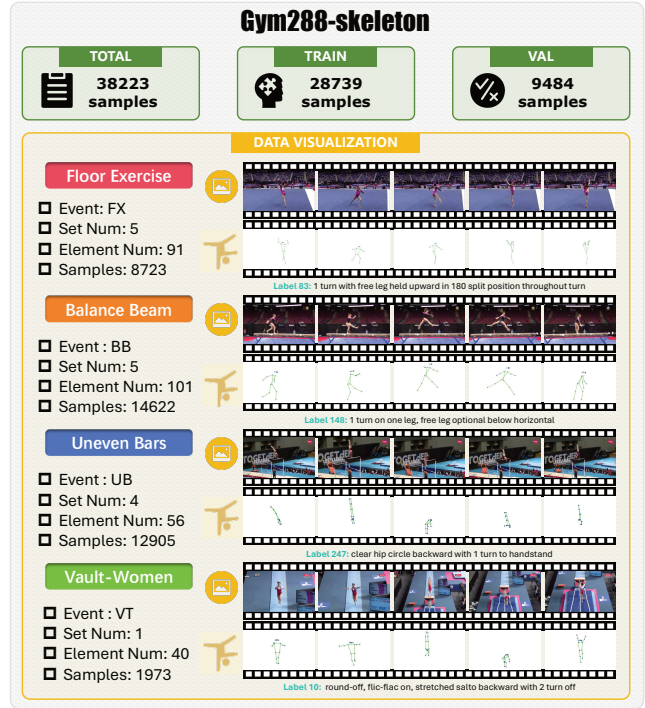


Figure 6: **Statistics and Visualized Analysis of our proposed Gym288-skeleton Dataset.** We present representative examples and a statistical comparison with the Gym99 Skeleton Dataset.

FineTec Training

During training, we use a batch size of 64. Input 2D skeletal joint data is processed through a pipeline involving pre-normalization and feature generation, followed by uniform sampling of sequences into 16-frame clips. The overall training duration is set for a maximum of 150 epochs. And this training step of Gym288-skeleton is conducted on a Linux (Ubuntu) machine with 4 NVIDIA 4090 GPUs within 5 hours.

B Model Details

Mask Strategies in the Context-aware Sequence Completion Module

To enhance robustness of FineTec and its ability to generalize across various data corruption types, it employs five distinct masking strategies on the reference sequence: 1) Random masking, which simulates sporadic data loss by dropping arbitrary frames; 2) Pattern-based masking, which replicates the specific mask pattern of the input query to train for structured gaps; 3) Left-side masking, which removes a continuous block from the beginning, analogous to a delayed motion capture start; 4) Right-side masking, which removes a block from the end, simulating early termination or forecasting tasks; and 5) Middle masking, which removes a central block to represent occlusions during an action. This diverse set of strategies ensures the Completion module is

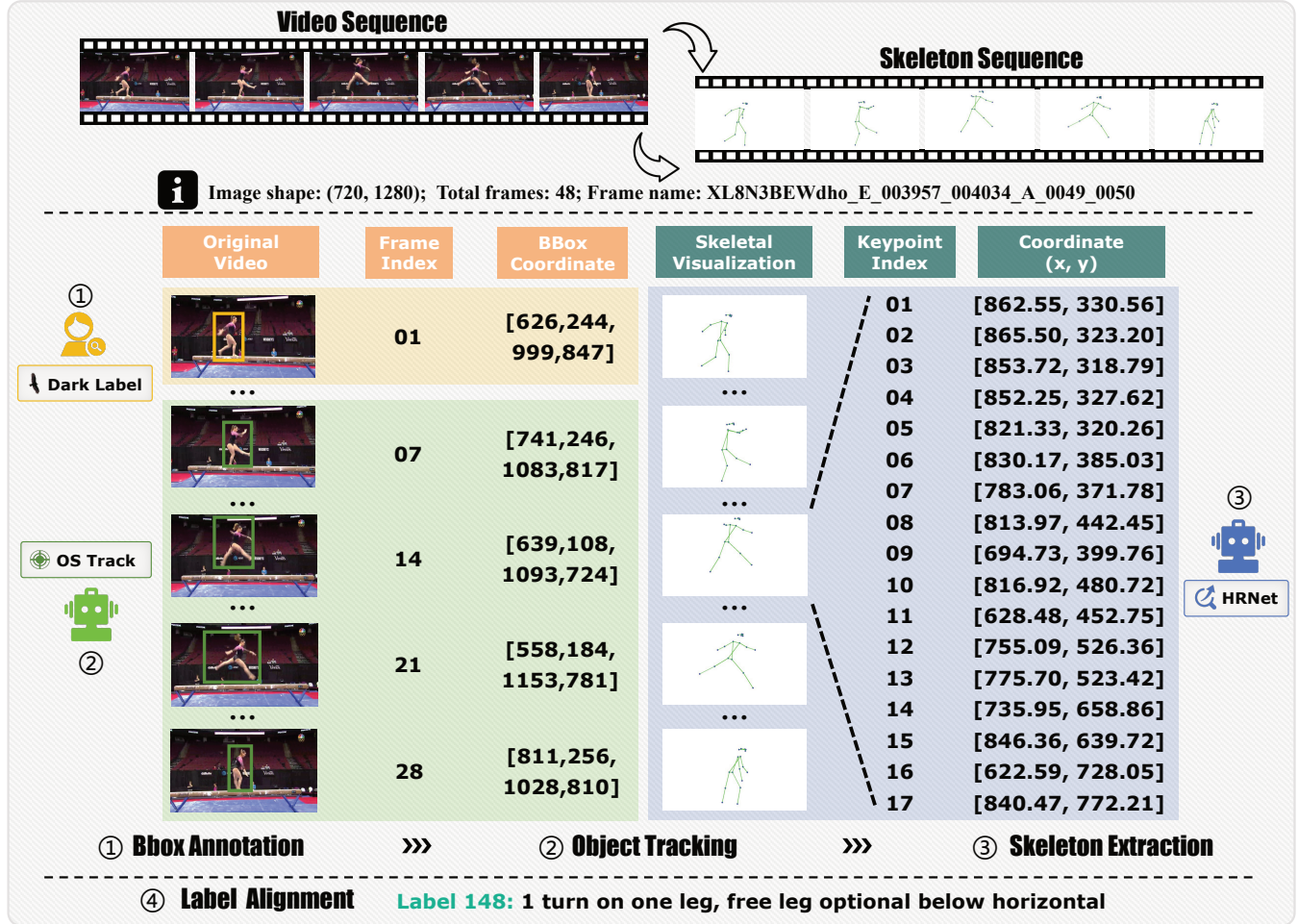


Figure 7: **Annotation Process of the Gym288 Skeleton Dataset on Label 148.** The skeleton comes from the elemental class “1 turn on one leg, free leg optional below horizontal”, the set class “switch leap (leap forward with leg change)” and the event class “Balance Beam”.

Table 7: **Comparison with state-of-the-art methods on UCF101.** Three levels of temporal corruption were set: minor, moderate, and severe. The evaluation metrics include top-1 accuracy and top-5 accuracy.

Method	UCF-Min.		UCF-Mod.		UCF-Sev.	
	Top-1	Top-5	Top-1	Top-5	Top-1	Top-5
ST-GCN <small>AAAI'18</small>	0.648	0.852	0.632	0.858	0.582	0.844
AAGCN <small>TIP'20</small>	0.634	0.851	0.636	0.861	0.638	0.843
FineTec (Ours)	0.652	0.861	0.638	0.859	0.621	0.847

trained on a wide range of missing data scenarios, significantly improving its performance and reliability for real-world motion in-painting tasks.

Augmentation Techniques in the Skeleton-based Spatial Decomposition Module

To enhance the ability of FineTec to capture fine-grained motion details, we employ both weak and strong augmentation strategies. Weak augmentation involves only temporal cropping to create slight temporal variations. The extreme augmentation pipeline, however, applies a diverse set of transformations to generate more challenging samples. These transformations can be broadly classified into three categories: (i) *Spatial augmentations*, which alter the skeletal structure within each frame through operations like random spatial flipping, Gaussian noise, axis masking, and bone rescaling; (ii) *Temporal augmentations*, which manipulate the sequence’s dynamics via random time flipping and interpolation; and (iii) *Spatio-temporal augmentations*, such as dropout, that introduce random occlusions across both space and time. This comprehensive strategy is designed to force FineTec to learn robust features that are invariant to significant appearance and motion variations, thereby enhancing

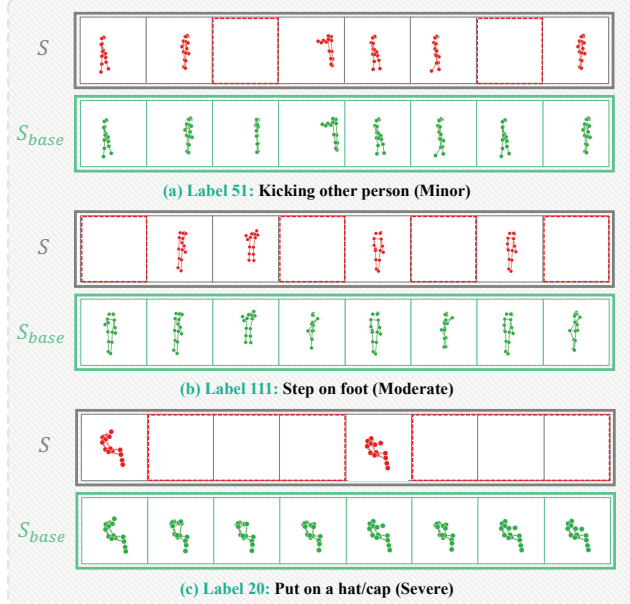


Figure 8: **Visualization of restoration on NTU-120-xsub.** Our Completion module produces complete and consistent skeletons using temporal-corrupted skeleton sequences.

its ability to distinguish between dynamic and static body parts.

C Gym288-skeleton Dataset

To facilitate a more rigorous analysis, we have augmented existing skeleton datasets by introducing a novel dataset annotated on the FineGym (Shao et al. 2020a) benchmark. This dataset is constructed by extending the open-source Gym99 dataset available in MMAction2. This section details our annotation pipeline, presents statistical analyses of the newly curated dataset, Gym288-skeleton, and includes illustrative visualization skeletons.

Formulation Pipeline

To ensure accurate target identification for skeleton extraction, we perform manual annotation. Specifically, bounding boxes for the primary athlete are manually annotated in the initial frame of 39,092 videos sourced from the FineGym dataset, which precisely define the targets for subsequent skeleton extraction. Following the identification of the initial target, the OS Track algorithm (Ye et al. 2022) is utilized to perform frame-by-frame object tracking throughout each video. This process yield the spatio-temporal trajectories of the primary athlete and generate the structured annotation files including frame-level skeletal coordinate information. With the HRNet skeleton annotator (Sun et al. 2019) and the above bounding boxes, we extract 17 human skeletal pose keypoints within each frame. And after data cleaning, we remove invalid or inaccurately identified data and curate a dataset comprising 38,223 skeletal action sequences of the primary subjects successfully. Finally, to determine the action category for each sequence, we match the video

filenames with the Gym288 classification index to assign a specific action label to each skeletal sequence, completing the creation of the Gym288-skeleton dataset.

Data Statistics and Visualization

Our Gym288 skeleton dataset contains a total of 38,223 skeleton sequence samples. These are categorized into four major disciplines: Balance Beam (BB), Floor Exercise (FX), Uneven Bars (UB), and Vault (VT), covering 288 fine-grained action classes, following FineGym (Shao et al. 2020a). The dataset is divided into 28,739 training samples and 9,484 validation samples. Gym288 is characterized by significant action diversity. For example, in Balance Beam, frequently occurring leap and turn movements include “split jump” (972 instances) and “switch leap to ring position” (350 instances). Similarly, in Uneven Bars, complex aerial movements on the bars such as “giant circle backward” (1,582 instances) and “transition flight between bars” (3,394 instances) are highly represented. Meanwhile, the Gym99 skeleton dataset comprises 29,005 skeleton sequence samples. It also covers the four major disciplines but includes only 99 action classes, with 19,121 training and 7,986 validation samples.

D Additional Illustration & Analysis

Elaboration on Euler-Lagrange Equations

In the main paper, we adopt the following standard form of the equations of motion in Lagrangian mechanics:

$$M(q_t)\ddot{q}_t + C(q_t, \dot{q}_t)\dot{q}_t + g(q_t) = \tau_t, \quad (18)$$

where $M(q_t)$ is the configuration-dependent inertia matrix characterizing the mass distribution of the system, $C(q_t, \dot{q}_t)\dot{q}_t$ encapsulates the Coriolis and centrifugal forces as functions of joint positions q_t and velocities \dot{q}_t , $g(q_t)$ represents the gravitational forces dependent on the configuration q_t , and τ_t denotes the vector of generalized forces, including joint torques and external forces. This formulation is derived from the classical Euler-Lagrange equations,

$$\frac{d}{dt} \frac{\partial L}{\partial \dot{q}^i}(t, q(t), \dot{q}(t)) - \frac{\partial L}{\partial q^i}(t, q(t), \dot{q}(t)) = \tau_t^i, \quad (19)$$

where the Lagrangian $L = T - V$ is defined by the kinetic energy $T = \frac{1}{2}\dot{q}^T M(q)\dot{q}$ and the potential energy $V = V(q)$. By computing the relevant derivatives,

$$\frac{\partial L}{\partial q^i} = -\frac{\partial V}{\partial q^i} + \frac{1}{2}\dot{q}^T \frac{\partial M(q)}{\partial q^i} \dot{q}, \quad (20)$$

$$\frac{d}{dt} \frac{\partial L}{\partial \dot{q}^i} = M_{ij}(q)\ddot{q}^j + \dot{q}^j \frac{\partial M_{ij}}{\partial q^k} \dot{q}^k, \quad (21)$$

and substituting into the Euler-Lagrange equation, we obtain

$$M(q)\ddot{q} + C(q, \dot{q})\dot{q} + g(q) = \tau, \quad (22)$$

where $C(q, \dot{q})\dot{q}$ collects the Coriolis and centrifugal terms, $g(q) = \frac{\partial V}{\partial q}$ is the gravitational force, and τ is the generalized force vector. This compact form is widely used in robotics and multibody dynamics for modeling and control.

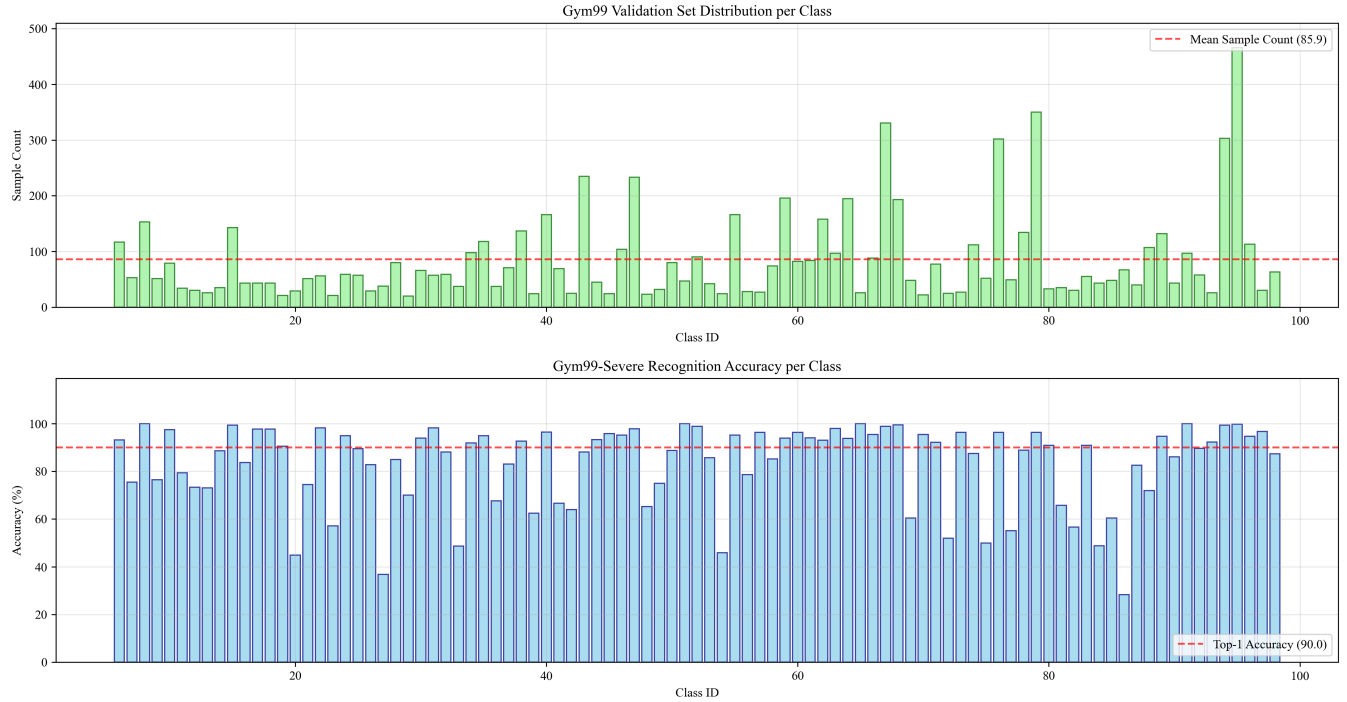


Figure 9: **Gym99-skeleton recognition Analysis.** The Top-1 accuracy is used. The upper figure illustrates the number of action sequences per class in the validation set, while the lower figure shows the corresponding per-class accuracy achieved by the FineTec model.

Visualization of Restoration on NTU-120-XSub

Figure 8 provides a qualitative analysis of skeleton restoration on the NTU-120-XSub dataset, a coarse-grained benchmark. Leveraging our Context-aware Sequence Completion module, we demonstrate the restoration of skeletal data under three corrupted scenarios across three representative action classes. For conciseness and due to page limitations, we visualize only 8 frames from the complete input sequence of 100 frames. The results on NTU-120 underscore the effectiveness of our module in achieving high-fidelity restoration across a diverse set of actions. This indicates our module’s strong generalization ability, making it a promising approach for various action recognition scenarios, including more complex, fine-grained datasets like FineGym. This robust performance underscores our capability to effectively reconstruct the spatio-temporal integrity of human movements, highlighting its strong generalization ability on datasets with varying levels of action granularity.

Analysis of Three Components in the Skeleton-based Spatial Decomposition Module

Figure 11 visualizes the three component sequences in Decomposition module, alongside their corresponding input skeleton sequence. To better elucidate how it leverages biological priors for fine-grained analysis within the skeletal space, we select three distinct action sets from the Gym288-skeleton dataset and present one representative element class (*i.e.*, label 43, 145, 271) from each for visualization. As can

Table 8: **Quantitative comparison between w/o ICL and MaskICL on the Gym99-Skeleton dataset.** All values are reported in position (MPJPE, N-MPJPE) or velocity error (MPJVE).

Severity	Method	MPJPE \downarrow	N-MPJPE \downarrow	MPJVE \downarrow
Min.	w/o ICL	0.115	0.103	0.114
	Ours	0.106	0.098	0.047
Mod.	w/o ICL	0.134	0.115	0.117
	Ours	0.119	0.109	0.085
Sev.	w/o ICL	0.169	0.140	0.121
	Ours	0.147	0.132	0.113

be observed, it effectively partitions the completed skeletons into DynamicUnits and StaticUnits, resulting in all sequences that are distinct from one another. This decomposition isolates the most discriminative body parts for action recognition, thereby amplifying the subtle yet crucial distinctions necessary for fine-grained analysis.

Experiment Results on the UCF101 Skeleton Dataset

To further assess the generalization and robustness of our proposed method, we conducted additional experiments on the UCF101 skeleton dataset. The sequence length is set to 16. As presented in Table 7, we compare our method, FineTec, with other baselines under three levels of temporal corruption: minor, moderate, and severe. FineTec achieves

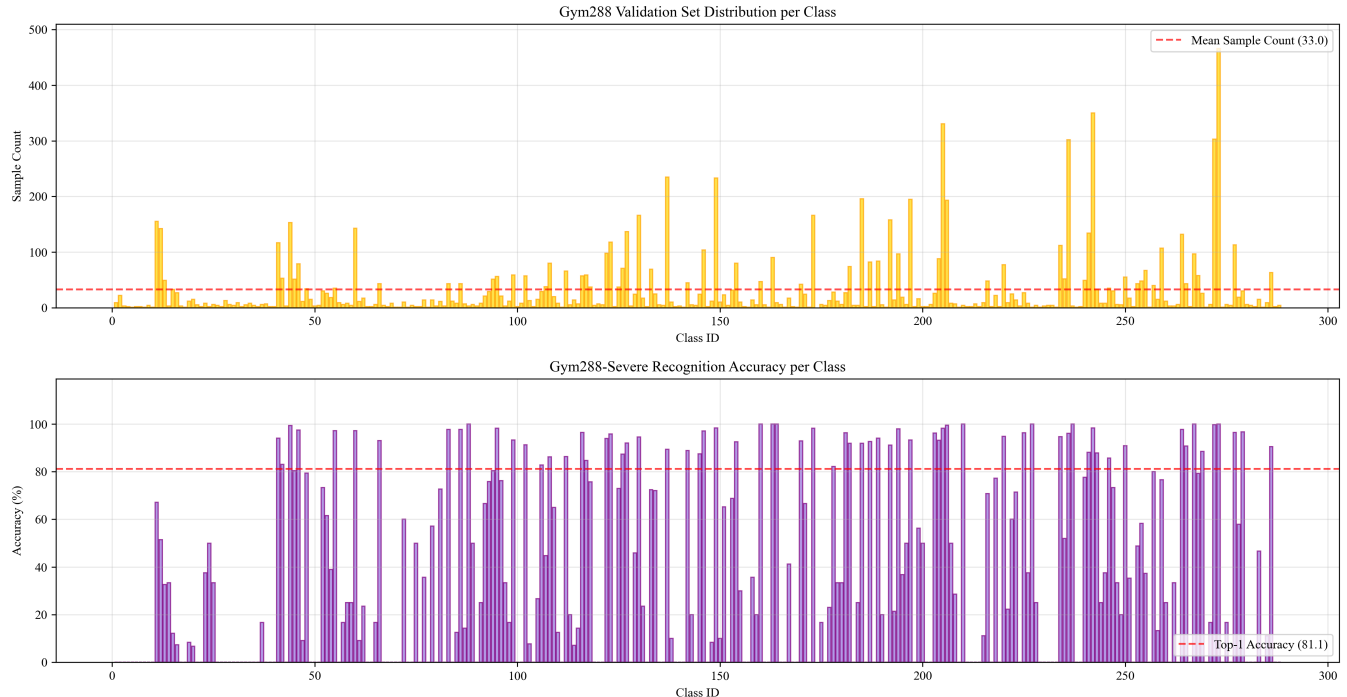


Figure 10: **Gym288-skeleton datasets recognition Analysis.** The Top-1 accuracy is used. The upper figure illustrates the number of action sequences per class in the validation set, while the lower figure shows the corresponding per-class accuracy achieved by the FineTec model.

Table 9: **Ablation Study on multi-GCNs and GCN types.** Three levels of temporal corruption were set: minor, moderate, and severe, performed on the Gym288-skeleton dataset. The evaluation metrics include top-1 accuracy and top-5 accuracy.

Method	G288-Min.		G288-Mod.		G288-Sev.	
	Top-1	Top-5	Top-1	Top-5	Top-1	Top-5
ST-GCN-based	0.778	0.923	0.756	0.913	0.723	0.892
Multi-GCNs	0.808	0.925	0.801	0.926	0.791	0.924
FineTec (Ours)	0.815	0.934	0.797	0.928	0.781	0.918

the highest Top-1 accuracy under both minor (0.652) and moderate (0.638) corruption levels. Even under severe corruption, our method maintains competitive performance, significantly outperforming ST-GCN. These results underscore the strong generalization ability and robustness of our method in large-scale action recognition scenarios.

Ablation on ICL scheme in Skeletal Restoration

As presented in Table 8, our module demonstrates superior performance against the baseline without in-context learning (w/o ICL) on the Gym99 Skeleton dataset. Specifically, even under severe perturbations (Sev), ours achieves notable reductions in position and velocity errors, with MPJPE

Table 10: **Model Complexity and Inference Speed.** Comparison of parameter counts (in millions) and inference time (in seconds) on the Gym288-skeleton dataset.

Model	Params (M)	Time (s)
ST-GCN (Yan, Xiong, and Lin 2018)	11.04	103
AAGCN (Shi et al. 2020)	13.42	186
CTRGCN (Chen et al. 2021)	5.31	220
FineTec (Ours)	10.51	169

decreasing from 0.169 to 0.147, N-MPJPE from 0.140 to 0.132, and MPJVE from 0.121 to 0.113. These results demonstrate that our designed masking mechanism and in-context learning effectively improve joint estimation accuracy and enhance the overall robustness of pose representation under temporal corruptions.

Analysis of Per-Class Prediction Performance on Gym99 and Gym288

As detailed in Figure 9 and Figure 10, we conducted a per-class performance analysis on the Gym99 and Gym288-skeleton datasets. On Gym99, our model achieves an overall accuracy of 89.99%. Notably, four categories (91, 51, 8, and 65) reach 100% accuracy, indicating robust feature extraction for these actions. However, some classes exhibit significantly lower performance, such as category 86 (*i.e.*, Uneven

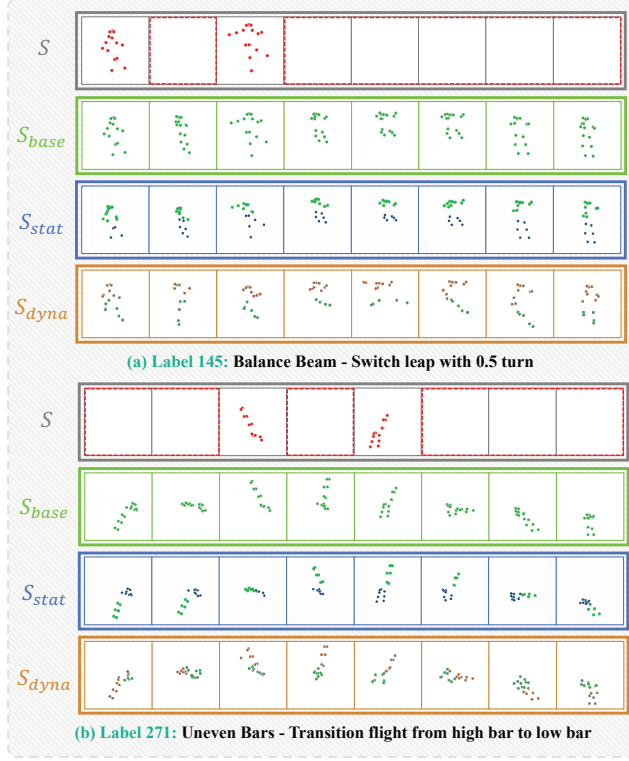


Figure 11: **Visualization of Three Components on the Gym288-skeleton Dataset in the Skeleton-based Spatial Decomposition.** Examples from three sets are visualized, with the temporal-corrupted skeleton inputs.

Bars: Clear pike circle backward to handstand) with only 28.36% accuracy. This discrepancy is likely attributable to a limited number of training samples (67 for category 86) and high inter-class similarity, as its motion patterns closely resemble those of categories 75 and 72, making differentiation challenging.

The Gym288-skeleton dataset poses a significant challenge, evidenced by a modest overall accuracy of 81.14%. This difficulty is attributable to several factors: 1) a three-fold increase in action categories to 288, which heightens inter-class similarity; 2) a severe class imbalance, leading to degraded performance on under-represented categories; and 3) the intrinsic complexity of actions, characterized by intricate spatiotemporal patterns and subtle variations that demand advanced modeling capabilities. Despite these hurdles, our proposed FineTec demonstrates robustness by achieving perfect accuracy on several well-populated classes. These findings validate Gym288-skeleton as a more rigorous benchmark for evaluating model generalization, owing to its fine-grained class distinctions and heightened action similarities.

Analysis of Multi-GCNs and GCN types

To investigate the impact of the GCN recognition module on our framework, we first evaluated a standard ST-GCN (Yan, Xiong, and Lin 2018) as the recognition backbone. Subse-

quently, we experimented with a Multi-GCN architecture, where six parallel GCNs individually process each of the six sequence types (*i.e.*, displacement S_{base} , S_{dyna} , S_{stat} and accelerate a_{base} , a_{dyna} , a_{stat}), followed by a fusion of the extracted features.

As shown in Table 9, the Multi-GCN approach consistently outperforms the single ST-GCN across all levels of temporal corruption on the Gym288-skeleton dataset. Specifically, for minor, moderate, and severe corruption, the Multi-GCN architecture improves the Top-1 accuracy by 3.0%, 4.5%, and a substantial 6.8%, respectively, compared to the standard ST-GCN. This trend highlights that dedicating separate GCN modules to different sequence types yields a more robust representation, with the performance advantage becoming more pronounced as the temporal data quality degrades. While our proposed FineTec method achieves the highest accuracy under minor corruption, the significant and consistent gains of the Multi-GCN architecture over the baseline ST-GCN validate its effectiveness in handling diverse and corrupted temporal sequences.

Comparison of Models’ Parameter Counts and Inference Time

As detailed in Table 10, our proposed model, FineTec, demonstrates a compelling balance between computational complexity and inference efficiency. With 10.51 million parameters, FineTec is more lightweight and faster than AAGCN, which has 13.42 million parameters and an inference time of 186 seconds. Notably, while CTRGCN features a smaller parameter count at 5.31 million, our model achieves a significantly faster inference time of 169 seconds compared to CTRGCN’s 220 seconds. This highlights FineTec’s effective design in achieving a favorable trade-off, ensuring competitive performance without excessive computational overhead.

Limitation and Future Works

While FineTec demonstrates promising results in fine-grained temporal defect detection by focusing on the explicit modeling of skeletal spatial and temporal dynamics, we acknowledge this as a preliminary step. There are several limitations and avenues for future research. 1) The primary innovation of this work lies in the explicit parsing of skeleton sequences, rather than a fundamental redesign of the GCN topology. A compelling future direction would be to embed the physical laws and biomechanical principles emphasized in this paper directly into the topological structure of GCNs. 2) Although this paper introduces a novel task, fine-grained temporal-corrupted action recognition, its scope is currently limited to the single task of action recognition. In our future work, we plan to leverage the proposed fine-grained explicit parsing methodology and apply it to a broader spectrum of skeleton-based tasks, such as skeleton completion and future frame prediction.